LETTER Communicated by Paul Bressloff

Interspike Interval Correlations, Memory, Adaptation, and Refractoriness in a Leaky Integrate-and-Fire Model with Threshold Fatigue

Maurice J. Chacron
mchacron@physics.uottawa.ca
Department of Physics, University of Ottawa, Ottawa, Canada K1N 6N5

Khashayar Pakdaman
pakdaman@u444.jussieu.fr
Inserm, U444, 75571 Paris Cedex 21, France

André Longtin
andre@physics.uottawa.ca
Department of Physics, University of Ottawa, Ottawa, Canada K1N 6N5

Neuronal adaptation as well as interdischarge interval correlations have been shown to be functionally important properties of physiological neurons. We explore the dynamics of a modified leaky integrate-and-fire (LIF) neuron, referred to as the LIF with threshold fatigue, and show that it reproduces these properties. In this model, the postdischarge threshold reset depends on the preceding sequence of discharge times. We show that in response to various classes of stimuli, namely, constant currents, step currents, white gaussian noise, and sinusoidal currents, the model exhibits new behavior compared with the standard LIF neuron. More precisely, (1) step currents lead to adaptation, that is, a progressive decrease of the discharge rate following the stimulus onset, while in the standard LIF, no such patterns are possible; (2) a saturation in the firing rate occurs in certain regimes, a behavior not seen in the LIF neuron; (3) interspike intervals of the noise-driven modified LIF under constant current are correlated in a way reminiscent of experimental observations, while those of the standard LIF are independent of one another; (4) the magnitude of the correlation coefficients decreases as a function of noise intensity; and (5) the dynamics of the sinusoidally forced modified LIF are described by iterates of an annulus map, an extension to the circle map dynamics displayed by the LIF model. Under certain conditions, this map can give rise to sensitivity to initial conditions and thus chaotic behavior.

1 Introduction

Since the seminal work of Adrian and Zotterman (1926), adaptation has been demonstrated to be a key property of neurons. For example, photoreceptor neurons have to cope with very different light intensities (e.g., day and night) and must adapt to each (Kuffler, Fitzhugh, & Barlow, 1957). Moreover, this adaptation can sometimes give rise to interspike interval (ISI) correlations in experimental recordings (Kuffler et al., 1957; Goldberg, Adrian, & Smith, 1964; Yamamoto & Nakahama, 1983; Teich & Lowen, 1994; Schäfer, Braun, Peters, & Bretschneider, 1995; Longtin & Racicot, 1998; Chacron, Longtin, St.-Hilaire, & Maler, 2000; Neiman & Russell, 2001; Liu & Wang, 2001; Brandman & Nelson, 2002).

Information-theoretic approaches have recently shown that neural information transfer can either increase or decrease as a result of correlations between spikes (Abbott & Dayan, 1999; Panzeri, Petersen, Schultz, Lebedev, & Diamond, 2001; Tiesinga, Fellous, José, & Sejnowski, 2002) or ISIs (Chacron, Longtin, & Maler, 2001a). Also, correlations between neuronal inputs can increase or decrease information transfer (Abbott & Dayan, 1999; Panzeri et al., 2001).

One prototype sensory system in which the role of ISI correlations has been addressed is the electrosensory system of weakly electric fish. Negative ISI correlations have been found in P-type electroreceptors (Longtin & Racicot, 1998). A modeling study of these receptors has further shown that these correlations enhance not only information transfer but signal detection as well (Chacron et al., 2001a). It is clear from those studies that ISI correlations depend on various biophysical model parameters, as well as on noise and periodic forcing. The goal of this article is to provide a foundation for understanding how ISI correlations arise from the interplay of these factors in the context of a simple model.

The leaky integrate-and-fire model (LIF) is one of the most elementary spiking models and has been widely used to gain a better understanding of information processing in neurons (see, e.g., Tuckwell, 1988). One feature that makes this model particularly suitable for theoretical analysis is that it is analytically tractable and retains two key neuronal properties of type I membranes: the all-or-none response and the postdischarge refractoriness. The tractability of the standard LIF is in part due to the fact that following a discharge, the dynamics of the LIF depends on only the present and future inputs. In other words, after each firing, the LIF has no memory of the past: inputs and discharge times prior to the last one bear no influence on the next discharge times. This property has been a key ingredient in the analysis of the response of the standard LIF to inputs such as sinusoidal current or white gaussian noise. Indeed, it allows the standard LIF to be described by iterates of orientation-preserving circle maps (Rescigno, Stein, Purple, & Popele, 1970; Keener, Hoppensteadt, & Rinzel, 1981; Coombes & Bressloff, 1999; Pakdaman, 2001). Moreover, the discharge times evoked by

gaussian white noise stimulation form a renewal process (for recent reviews on the noisy LIF, see Lansky & Sato, 1999; Ricciardi, Di Crescenzo, Giornio, & Nobile, 1999; Pakdaman, Tanabe, & Shimokawa, 2001).

The lack of memory about past discharges, which constitutes an advantage in the theoretical analysis of the standard LIF, is also one of the shortcomings of this model. Indeed, this property can eliminate the correlation between successive interspike intervals (ISIs) of the LIF. For instance, the ISIs evoked by additive gaussian white noise stimulation of this model are independent from one another. As mentioned, this is not the case experimentally for many neurons. Moreover, the LIF model assumes that the threshold to firing is constant in time. There is experimental evidence that the threshold for firing is not constant but depends on the past spiking history of the neuron (Azouz & Gray, 1999). Thus, a physiologically plausible modification to the LIF neuron would be to make the threshold a dynamical variable also.

In this article, we study a modified LIF neuron in which the threshold is a dynamical variable that models threshold fatigue after an action potential. Using step currents as stimuli, we show that the model can give rise to adaptation (i.e., a gradual change in firing rate), a feature that is absent from the standard LIF model. Under certain conditions, we show that the threshold fatigue can lead to a saturation in the firing rate of the neuron as the depolarizing current is increased. This feature is also absent from the LIF model, where the firing rate diverges as a function of input current. We then show that the modified LIF incorporating threshold fatigue can reproduce ISI correlations similar to those found in experimental recordings. The choice of the threshold dynamics is guided by previous observations that ISI correlations can result from the progressive accumulation of refractory effects (Stein, 1965; Weiss, 1966; Geisler & Goldberg, 1966; Holden, 1976; Gerstner & van Hemmen, 1992; Chacron et al., 2000, 2001a; Chacron, Longtin, & Maler, 2001b; Liu & Wang, 2001). If the neuron fires two spikes in a relatively short time interval, then the next action potential usually occurs after a longer time interval. Implementing threshold fatigue, that is, decreasing excitability during high-frequency firing, in the LIF should thus be a candidate for increasing the ISI correlations in a satisfactory way. Our investigations provide another confirmation of this point. Although more detailed ionic models of neurons such as the Hodgkin-Huxley model (Hodgkin & Huxley, 1952) are capable of adaptation and ISI correlations with the addition of suitable ionic channels, such models seldom are analytically tractable due to their complexity. In contrast, our model retains enough of the simplicity of the LIF model to remain analytically tractable for the most part.

Various integrate-and-fire-like models with mechanisms analogous to threshold fatigue have been previously used—for instance:

- In the analysis of mutually inhibiting neuronal models (Reiss, 1962; Wilson & Waldron, 1968: for an account of these studies, see MacGregor & Lewis, 1977)

- A stochastic model where an inhibitory conductance is being reset to a value dependent on past history to mimic the possible summation of hyperpolarizing afterpotentials following each discharge (Geisler & Goldberg, 1966; Wehmier, Dong, Koch, & van Essen, 1989; Treves, 1996; Liu & Wang, 2001)
- Periodically and irregularly forced neuronal models (Segundo, Perkel, Wyman, Hegstad, & Moore, 1968)
- Self-exciting models and interacting excitatory assemblies (Vibert, Pakdaman, & Azmy, 1994; Pakdaman & Vibert, 1995; Pakdaman, Vibert, Boussard, & Azmy, 1996)
- An LIF model in which the threshold decayed exponentially and was incremented by a fixed amount immediately after an action potential (Geisler & Goldberg, 1966; Holden, 1976; Chacron et al., 2000, 2001a, 2001b; Liu & Wang, 2001)

Although the model used in this study bears similarities with previous ones, one key difference resides in the introduction of a memory parameter to adjust the level of fatigue. Indeed, previous studies dealt with neuron models with a fixed level of fatigue, whereas this one is concerned with a systematic analysis of the influence of this factor. This program is carried out in three stages involving the description of the response of the modified LIF to (1) constant and step current stimulation, (2) white gaussian noise, and (3) sinusoidal forcing. The first two stages are concerned with adaptation and the ISI correlations due to fatigue. The last stage examines how these factors affect the response of the modified model to other inputs. The particular selection of sinusoidal forcing is motivated by its relevance for understanding information processing in extrinsically forced neurons (Chacron et al., 2000). Furthermore, comparison of our results with the extensive studies of sinusoidally forced LIFs and their variants (Rescigno et al., 1970; Glass & Mackey, 1979; Keener et al., 1981; Alstrøm & Levinsen, 1988; Coombes, 1999; Coombes & Bressloff, 1999; Pakdaman, 2001) provides the basis for the determination of specific contributions of threshold fatigue to the dynamics of the model.

2 The Model

We consider the model given by the following equations and firing rule:

$$\frac{dv}{dt} = -v/\tau_v + I(t) \quad \text{if } v(t) < s(t), \tag{2.1}$$

$$\frac{ds}{dt} = \frac{s_r - s}{\tau_s} \quad \text{if } v(t) < s(t), \tag{2.2}$$

$$v(t^+) = v_0 \quad \text{if } v(t) = s(t) \tag{2.3}$$

$$s(t^+) = s_0 + W(s(t), \alpha) \quad \text{if } v(t) = s(t), \tag{2.4}$$

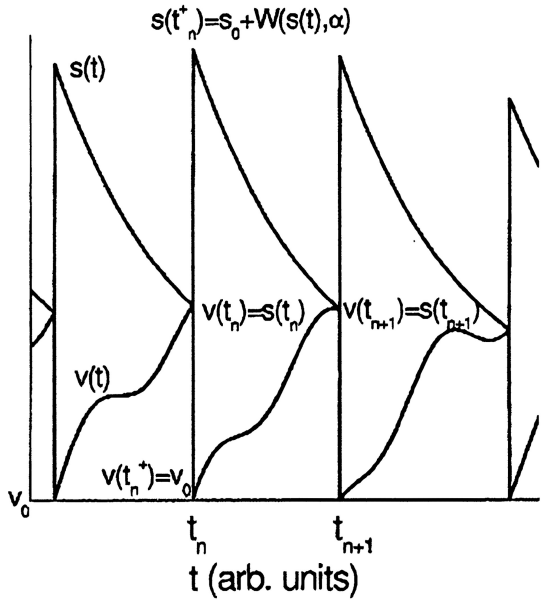

Figure 1: Voltage (black solid line) and threshold (gray solid line) time series obtained with the model. An action potential occurs when voltage and threshold are equal. The firing times t_n thus satisfy $v(t_n) = s(t_n)$. Immediately after an action potential, the voltage is reset to zero while the threshold is set to a value $s(t_n^+) = s_0 + W(s(t_n), \alpha)$.

where v is the voltage, s is the threshold, $I(t)$ is the stimulation current, τ_v and τ_s are the time constants for voltage and threshold, respectively, and s_r is the value at which the threshold stabilizes in the absence of firing. Firing occurs when the voltage reaches the threshold. Following this, the voltage is reset to v_0 (see equation 2.3), and the threshold is set to $s(t^+) = s_0 + W(s(t), \alpha)$, where s_0 is a parameter and W is a monotically increasing function of s and α with $W(s, 0) = 0$. α is a positive parameter controlling the memory in the model. We will mostly look at the case $W(s, \alpha) = W_1(s, \alpha) \equiv \alpha s$, but other nonlinear forms could be used for W. Throughout, we assume that $v_0 \leq 0 < s_r \leq s_0$. The model dynamics are graphically illustrated in Figure 1.

Equation 2.4 with $W = W_1$ represents threshold fatigue, with α being the memory parameter. Indeed, when $\alpha = 0$, the threshold value immediately after a discharge is independent of the threshold value at that discharge, so that future discharges bear no memory of the firing history. The case where $\alpha = 0$ and $s_0 = s_r$ corresponds to the standard LIF with constant threshold. Conversely, when $W = W_1$ and $\alpha = 1$, one recovers the threshold fatigue

implemented in previous studies, that is, after each discharge, the threshold is raised by a fixed amount s_0 (Segundo et al., 1968; Vibert et al., 1994; Pakdaman & Vibert, 1995; Pakdaman et al., 1996; Chacron et al., 2000, 2001a, 2001b; Liu & Wang, 2001). Other models used a conductance that was decremented by a fixed amount immediately after an action potential to achieve similar effects (Wehmeier et al., 1989; Treves, 1996; Liu & Wang, 2001). Liu and Wang (2001) have shown that the latter approach gave qualitatively similar results to our model with $W = W_1$ and $\alpha = 1$. Previous studies were thus limited to the case $\alpha = 1$.

Generally, increasing α from zero corresponds to increasing the degree of fatigue in the model and, consequently, its dependence on its past. The following sections examine how this parameter affects the correlation between consecutive ISIs and the response of the model to various stimuli.

3 Results

3.1 Constant and Step Current Stimulation. Throughout this section, we assume $W = W_1$ and that $I(t) = \mu$ is constant. Two situations arise in response to such stimuli. When $\mu\tau_v < s_r$, the stimulus is subthreshold, the membrane potential $v(t)$ stabilizes at $\mu\tau_v$, and no firing occurs. Conversely, when $\mu\tau_v > s_r$, the model generates sustained firing. The remainder of this section analyzes the corresponding discharge pattern. This is done through the construction of a map relating consecutive postdischarge threshold values. Let $v(u)$ be the solution to equation 2.1 with $v(0) = v_0$, and let $s(u, S)$ be the solution to equation 2.2 with $s(0, S) = S$. These are given by

$$v(u) = (v_0 - \mu\tau_v)e^{-u/\tau_v} + \mu\tau_v \tag{3.1}$$

$$s(u, S) = (S - s_r)e^{-u/\tau_s} + s_r. \tag{3.2}$$

Let us assume that a discharge occurred at time t_n and resulted in the postdischarge threshold $s(t_n^+) \equiv S_n^+$. The next firing takes place after a time interval $\Delta_{n+1} \equiv t_{n+1} - t_n$ such that

$$s(\Delta_{n+1}, S_n^+) = v(\Delta_{n+1}) \text{ and } s(u, S_n^+) > v(u) \text{ for all } 0 \leq u < \Delta_{n+1}. \tag{3.3}$$

This firing yields the postdischarge threshold S_{n+1}^+ at time t_{n+1}^+:

$$S_{n+1}^+ = s_0 + \alpha s(\Delta_{n+1}, S_n^+) \tag{3.4}$$

$$= s_0 + \alpha v(\Delta_{n+1}) \tag{3.5}$$

$$= s_0 + \alpha[(S_n^+ - s_r)e^{-\Delta_{n+1}/\tau_s} + s_r]. \tag{3.6}$$

From these equations, the relation between the nth and $n+1$th ISIs Δ_n and Δ_{n+1} is readily derived as:

$$\Delta_n = -\tau_v \ln \left\{ \frac{\begin{array}{c}[(v_0 - \mu\tau_v)e^{-\Delta_{n+1}/\tau_v} + \mu\tau_v - s_r] \\ \times e^{\Delta_{n+1}/\tau_s} + s_r - s_0 - \alpha\mu\tau_v\end{array}}{\alpha(v_0 - \mu\tau_v)} \right\}. \tag{3.7}$$

While equation 3.7 can be used to discuss the relation between successive ISIs, we prefer to focus on the relation between successive values of the postdischarge threshold. Indeed, for constant stimulation, from the ISI Δ_n one can unambiguously derive S_n^+, the nth postdischarge threshold, and conversely, given S_n^+, there is a unique ISI Δ_n, so that using either the ISIs or the postdischarge thresholds yields the same information about the dynamics of the model. However, for the class of stimuli treated in section 3.2, this is not necessarily so; different values of S_n may yield the same Δ_n. This in turn makes it more difficult to obtain the relation between Δ_n and Δ_{n+1}. For this reason, the following paragraphs describe the relation between S_n^+ and S_{n+1}^+.

Equation 3.3 uniquely defines $\Delta_{n+1} = \Delta_{n+1}(S_n^+)$ as a function of S_n^+, so that we can rewrite equation 3.4 as

$$S_{n+1}^+ = s_0 + \alpha s(\Delta_{n+1}(S_n^+), S_n^+) \equiv F(S_n^+). \tag{3.8}$$

This relation implies that the postdischarge threshold S_n^+ after the nth firing entirely determines the next postdischarge firing S_{n+1}^+. In other words, the dynamics of the LIF with threshold fatigue receiving a constant stimulation is determined by the iterates of the map F. This map is defined on the interval $[s_0 + \alpha s_r, +\infty)$. In general, $\Delta(S)$, and consequently $F(S)$ cannot be explicitly written in closed form because equation 3.3 cannot be solved analytically for arbitrary τ_s. However, the geometrical properties of F that determine the behavior of the sequence $\{S_n^+\}$ can be determined without such knowledge.

For fixed u, the function $s(u, S)$ is monotonic increasing, so that if $S > S'$, then $s(u, S)$ cannot intersect the voltage prior to $s(u, S')$. In other words, $S > S'$ implies that $\Delta(S) > \Delta(S')$, which means that the larger the postdischarge threshold is, the longer the following interspike interval. Given that $v_0 \leq 0 < \mu\tau_v$ (the postdischarge potential is reset below the resting voltage) and that $v(u)$ is monotonic increasing, we have that $\Delta(S) > \Delta(S')$ implies $v(\Delta(S)) > v(\Delta(S'))$. This relation together with equation 3.5 and $\alpha > 0$ yields that $F(S) > F(S')$ whenever $S > S'$, that is, F is monotonic increasing. This, combined with the observation that $F(s_0 + \alpha s_r) > s_0 + \alpha s_r$, and $F(S) \to s_0 + \alpha\mu\tau_v$ as $S \to +\infty$, ensures that for any $S_1^+ \in [s_0 + \alpha s_r, +\infty)$, the sequence S_n^+ is either increasing or decreasing and converges to some value in $[s_0 + \alpha s_r, s_0 + \alpha\mu\tau_v]$. Finally, all sequences converge to the same value, that is, F has a unique fixed point, because F is concave. This property comes from the fact

that $S \to s(u, S)$ is contracting, that is, $|s(u, S) - s(u, S')| = \exp(-u/\tau_s)|S - S'| < |S - S'|$ for $u > 0$, and $v(u)$ is concave, so that F', the derivative of F is monotonic decreasing.

In summary, we have established that the dynamics of the modified LIF with constant current is governed by

$$S_{n+1}^{+} = F(S_n^{+}), \tag{3.9}$$

where F, which maps $[s_0 + \alpha s_r, +\infty)$ onto $[s_0 + \alpha s_r, s_0 + \alpha\mu\tau_v)$, is a concave monotonic increasing function with a unique fixed point that we denote by S^*. Thus, for all $S_1 < S^*$, the sequence S_n^{+} increases and converges to S^*, and, conversely, for all $S_1^{+} > S^*$, the sequence S_n^{+} decreases toward S^*.

The first consequence of the above result is that in response to a constant stimulation, the modified LIF stabilizes at a periodic firing with constant interspike intervals Δ^* given by

$$\Delta^* = \tau_v \ln\left[\frac{\alpha(v_0 - \mu\tau_v)}{S^* - s_0 - \alpha\mu\tau_v}\right]. \tag{3.10}$$

We remark that since $\Delta(S)$ is independent of α, the map F defined in equation 3.8 is an increasing function of α. A consequence of this observation is that the value of equilibrium postdischarge S^* increases with α. Given that $\Delta^* = \Delta(S^*)$, the firing period also increases with α. In other words, the stationary firing slows down as the factor representing threshold fatigue increases.

We now study how Δ^* varies with the input current μ. Although it is not possible in general to solve equation 3.7 to find Δ^* as a function of μ, it is possible to solve for μ as a function of Δ^*. We get

$$\mu(\Delta^*) = \frac{-s_0 + s_r - s_r e^{\Delta^*/\tau_s} + v_0 e^{\Delta^*/\tau_s} e^{-\Delta^*/\tau_v} - \alpha v_0 e^{-\Delta^*/\tau_v}}{\tau_v(\alpha - e^{\Delta^*/\tau_s} + e^{\Delta^*/\tau_s} e^{-\Delta^*/\tau_v} - \alpha e^{-\Delta^*/\tau_v})}. \tag{3.11}$$

The derivative of μ with respect to Δ^* is always negative under the assumptions $v_0 \le 0 < s_r \le s_0$, $\alpha > 0$, and $\Delta^* \ge \tau_s \ln(\alpha)$. We will now show that the ISI Δ^* can never be less than $\tau_s \ln(\alpha)$.

If $\alpha \le 1$, this condition is trivially satisfied as $\tau_s \ln(\alpha) \le 0$ and $\Delta^* > 0$. We thus concentrate on the case $\alpha > 1$. The denominator of equation 3.11 is zero when $\Delta^* = \tau_s \ln(\alpha)$, so the function $\mu(\Delta^*)$ has a pole at this point. Since the function $\mu(\Delta^*)$ is monotonically decreasing and continuously differentiable on the range $(\tau_s \ln(\alpha), +\infty)$ and $\lim_{\Delta^* \to +\infty} \mu(\Delta^*) = s_r/\tau_v > 0$, we have that $\lim_{\Delta^* \to \tau_s \ln(\alpha)} \mu(\Delta^*) = +\infty$. Thus, as we increase μ from s_r/τ_v to $+\infty$, the ISI Δ^* decreases from ∞ to $\tau_s \ln(\alpha)$. The ISI Δ^* can thus never be lesser than $\tau_s \ln(\alpha)$ if $\alpha > 1$. This has important implications for the model dynamics. In particular, it implies that the stationary ISI Δ^* remains greater than $\tau_s \ln(\alpha)$ as we increase μ to arbitrarily large values.

Moreover, the fact that $\mu(\Delta^*)$ is a decreasing function of Δ^* implies that the firing frequency $1/\Delta^*$ is always a monotonically increasing function of μ. However, if $\alpha > 1$, the firing frequency will saturate to a finite value given by $(\tau_s \ln(\alpha))^{-1}$. As mentioned above, this feature is absent from the LIF model ($\alpha = 0, s_r = s_0$) where the firing rate diverges as a function of the input current. This type of behavior is commonly seen in experimental recordings and is usually associated with absolute refractoriness. Note, however, that the saturation in firing rate does not imply that an absolute refractory period is present in the model. Indeed, the model can give rise to an ISI smaller than $\tau_s \ln(\alpha)$ following a sufficiently high current pulse or step (see Figure 2C). Thus, we show that even in the absence of an absolute refractory period in the classical sense, threshold fatigue can give rise to a saturation in the firing frequency under constant current input. This has important implications; it may be that the saturation in firing rate seen in experimental recordings under constant depolarizing current is due to threshold fatigue rather than the absolute refractory period of the neuron.

A modification $\delta\mu$ of the value of μ leads to a transient modification of the discharge rate of the model. Notably, when $\delta\mu > 0$, the sequence S_n increases from the previous value of S^* toward the new value, resulting in a progressive lengthening of intervals to the new stationary ISI. Note that this ISI will be shorter than the old one. If initially $\mu\tau_v < s_r$ is subthreshold and the new value is suprathreshold, the transient regime in which the ISIs are shorter than in the stationary regime corresponds to neuronal adaptation, that is, a transient frequency increase at the onset of stimulation.

The above results hold for all $\alpha > 0$. However, some distinctions exist between the different values of α that clarify the role of this parameter. One point is that for $\alpha \leq 1$, the map F is contracting, that is, $F'(S) < 1$ for all S, but this is not necessarily so for $\alpha > 1$, where the map may be expanding in some intervals of S. This means that the effects such as discharge rate adaptation tend to be more pronounced in maps with large α than in those with small α. Figure 2A shows the response of the model to a step current going from the subthreshold regime to the suprathreshold regime. Note that the ISIs progressively increase to the new equilibrium value as is seen in experimental recordings (Adrian & Zotterman, 1926). Figure 2B shows the response of the model when the value of the current before the step was set to be in the suprathreshold regime with all other parameters unchanged. Figure 2C shows the response of the model to the same step as in Figure 2B but with α increased. Note the faster rate of adaptation. The rate at which the model adapts to a step current can thus be varied by changing the parameter α.

3.2 Gaussian White Noise Stimulation. Throughout this section, we assume $W = W_1$ and that $I(t) = \mu + \sigma\xi(t)$ where μ is constant and ξ is white gaussian noise with unit intensity. In this situation, the voltage and threshold of the model are stochastic processes that depend on the particular noise

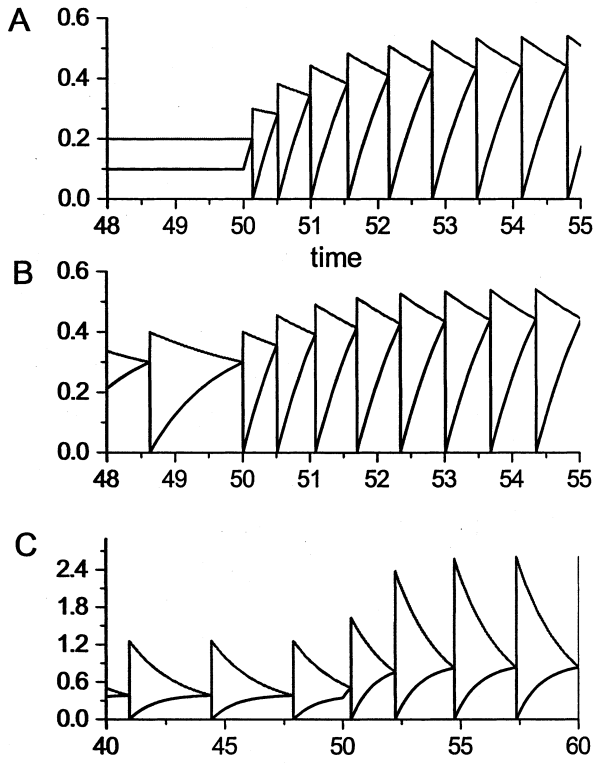

Figure 2: Response of the model to a step increase in current. (A) The current goes from subthreshold ($\mu = 0.1$) to suprathreshold ($\mu = 0.9$) at $t = 50$. Note the adaptation in the threshold and the progressive lengthening of ISIs to the new equilibrium value. Parameter values used were $\tau_s = 2$, $\tau_v = 1$, $\alpha = 1$, $s_r = 0.2$, $s_0 = 0.1$, $v_0 = 0$. (B) The current goes from $\mu = 0.4$ to $\mu = 0.9$ with all other parameters unchanged. (C) Illustration of the effects of increased α. μ goes from 0.4 to 0.9 but $\alpha = 10$ with all other parameters unchanged. Note the increased rate of adaptation.

realization. The interspike intervals are defined as the first passage times (FPTs) of the voltage through the threshold.

When $\alpha = 0$, that is, in the absence of threshold fatigue, the ISIs are independent and identically distributed random variables. We denote by $g(t \mid s_0)$ the probability density function (pdf) of these variables, that is, the function $g(t \mid s_0)$ is the FPT pdf of the Ornstein-Uhlenbeck process η,

$$\frac{d\eta}{dt} = -\eta/\tau_v + \mu + \sigma\xi(t) \text{ with } \eta(0) = \eta_0, \tag{3.12}$$

through the threshold $s(t) = (s_0 - s_r)\exp(-t/\tau_s) + s_r$. The FPT pdf g contains all information concerning the point process formed by the discharge times of the model.

When $\alpha > 0$, the description of the discharge times needs to take into account the variations in the postdischarge time threshold. In the same way as for constant stimulation, the key point to the description of the behavior of the model is in establishing the relation between consecutive postdischarge thresholds. In this case, given that the stimulation is noise, the description involves the construction of a Markov chain rather than a map. This is detailed in the following.

The conditional pdf of S_{n+1}^+ given S_n^+ can be written as

$$\Pi_1(u \mid S_n^+) = \frac{\tau_s}{u - s_0 - \alpha s_r} g\left[\tau_s \ln \frac{\alpha(S_n^+ - s_r)}{u - s_0 - \alpha s_r} \mid S_n^+\right], \tag{3.13}$$

where as before g represents the FPT pdf of the Ornstein-Uhlenbeck process, equation 3.12, through the threshold $s(t, S_n^+) = (S_n^+ - s_r)\exp(-t/\tau_s) + s_r$.

The pdf Π_1 defines the first-order transition probabilities of an irreducible Markov chain. We denote by $h^*(S)$ the stationary distribution of this chain—in other words, in the long run, the probability for the postdischarge threshold to take a value within $(S, S + dS)$ is given by $h^*(S)dS$. The characteristics of the point process formed by the discharge times of the model are then defined in terms of this stationary distribution together with g and Π_1. For instance, the pdf of ISI distribution $g^*(t)$ is given by

$$g^*(t) = \int g(t \mid S)h^*(S)\, dS. \tag{3.14}$$

We are interested in the serial correlation coefficient of ISIs defined by

$$\rho_p = \frac{\langle \Delta_n \Delta_{n+p} \rangle - \langle \Delta_n \rangle^2}{\langle \Delta_n^2 \rangle - \langle \Delta_n \rangle^2}, \tag{3.15}$$

where $\langle \Delta_n \Delta_{n+p} \rangle$, $\langle \Delta_n^2 \rangle$, and $\langle \Delta_n \rangle$ are the expectations of $\Delta_n \Delta_{n+p}$, Δ_n^2, and Δ_n, respectively.

For n large, the last two quantities are determined by $\langle \Delta_n \rangle = \int t g^*(t)\, dt$ and $\langle \Delta_n^2 \rangle = \int t^2 g^*(t)\, dt$. For the first term—the expectation of the product of two intervals—we first consider the case where n is large and $p = 1$. Given S_n^+, the postdischarge threshold after the nth discharge, the ISI between the nth and $n + 1$th firings, that is, Δ_n, is distributed according to $g(t \mid S_n^+)$. The knowledge of S_n^+ and Δ_n uniquely determines S_{n+1}^+ as

$$S_{n+1}^+ = (S_n^+ - s_r)e^{-\Delta_n/\tau_s} + s_r = f(S_n^+, \Delta_n). \tag{3.16}$$

This knowledge in turn yields that the ISI between the $n + 1$th and $n + 2$th firings, Δ_{n+1}, has pdf $g(t \mid S_{n+1}^+) = g(t \mid f(S_n^+, \Delta_n))$. Combining these with

the fact that for n large, S_n^+ is distributed according to h^* yields

$$\langle \Delta_n \Delta_{n+1} \rangle = \int_S \int_\Delta \int_{\Delta'} \Delta\Delta' \times g[\Delta' \mid f(S, \Delta)] \times g[\Delta \mid S] \times h^*(S)\, d\Delta'\, d\Delta\, dS. \tag{3.17}$$

In a similar way, we derive

$$\langle \Delta_n \Delta_{n+p} \rangle = \int_S \int_\Delta \int_{S'} \int_{\Delta'} \Delta\Delta' \times g[\Delta' \mid S'] \Pi_{p-1}[S' \mid f(S, \Delta)] \times g[\Delta \mid S] \times h^*(S)\, d\Delta'\, dS'\, d\Delta\, dS, \tag{3.18}$$

where Π_{p-1} is the $p-1$th transition pdf, that is, $\Pi_0(u \mid S) = \delta(u - S)$ the Dirac function at S, and $\Pi_{k+1}(u \mid S) = \int_{S'} \Pi_1(u \mid S')\Pi_k(S' \mid S)dS'$.

In the absence of threshold fatigue, when $\alpha = 0$, the postdischarge threshold is a fixed value s_0, so that $\Pi_1(u \mid S) = \delta(u - s_0)$, $h^*(S) = \delta(S - s_0)$, and $f(S, \Delta) = s_0$. Substituting these into equation 3.18 yields that for $p \geq 1$, $\langle \Delta_n \Delta_{n+p} \rangle = \langle \Delta_n \rangle \langle \Delta_{n+p} \rangle$ and consequently that $\rho_p = 0$.

The analysis of the previous paragraphs establishes that the response to gaussian white noise of the modified LIF with threshold fatigue is not described by a renewal process when $\alpha > 0$. This is in contrast with the standard LIF whose response to white gaussian noise can be described by a renewal process. It also revealed that the modified model with noisy forcing was characterized by a Markov chain relating consecutive postdischarge thresholds. Finally, it showed that the dependence of a postdischarge threshold on the previous value induces correlation between ISIs. Once it is theoretically established that ISIs of the modified model are correlated with one another, we examine the nature of this dependence. For this purpose, rather than using the integral expressions obtained previously, it is appropriate to use numerical simulations of the model. Indeed, the integrals require the computation of the FPT pdf of the Ornstein-Uhlenbeck process through an exponential boundary. Given that no general analytical expression is available for this quantity, derivation of the correlation from the integrals can be computationally more demanding than estimating the same quantities from simulations.

Figure 3A shows the ISI distribution $g^*(t)$ obtained when the system is driven by gaussian white noise for $\alpha = 1$, and Figure 3B shows the ISI correlation coefficients ρ_p. The estimated ρ_1 is negative. Serial correlation coefficients at higher lags are close to zero, illustrating the rapid return of the system to equilibrium. The fact that ρ_1 is negative and that it is the only coefficient substantially different from zero implies that ISIs shorter (longer) than average will be followed by ISIs longer (shorter) than average. Figure 3C shows the ISI distribution obtained for $\alpha = 4$. We can see that increasing α increases the mean ISI. Also, the magnitude of the coefficient ρ_1

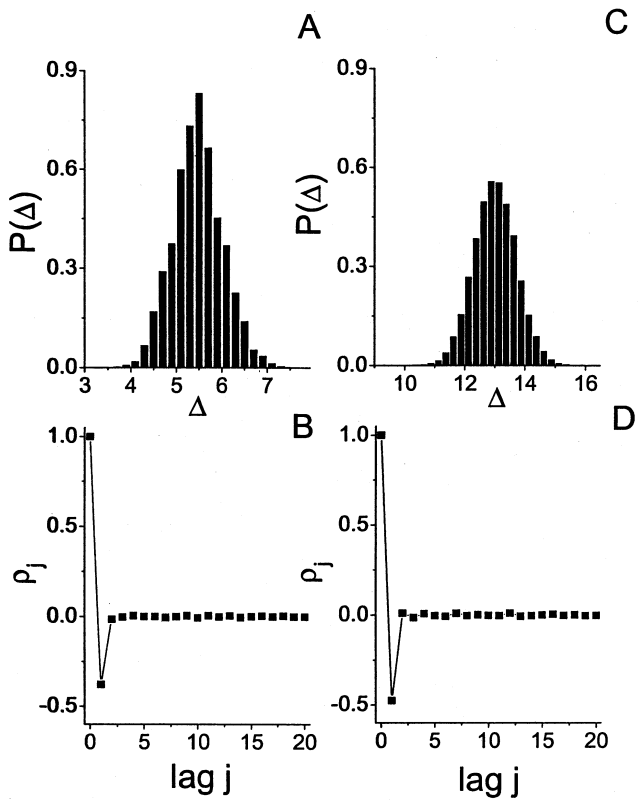

Figure 3: (A) ISI distribution obtained for $\alpha = 1$ in the presence of gaussian white noise of standard deviation 0.1. (B) Correlation coefficients ρ_j as a function of lag. Note that only $\rho_1 = -0.38$ is negative and that all coefficients are zero for higher lags. (C) ISI distribution obtained for $\alpha = 4$. (D) Correlation coefficients. Note that $\rho_1 = -0.48$ is lower than for $\alpha = 1$. Other parameter values were $\tau_s = 8$, $\tau_v = 1$, $\mu = 1$, $s_r = 0$, $s_0 = 1$.

increases with α, which is consistent with the predictions that more memory will give rise to more pronounced ISI correlations.

The magnitude of the serial correlation coefficient at lag one depends on the slope of the map $S \rightarrow F(S)$ and on the strength of the noise. For high noise intensity, it is expected that the noise will wash out the correlations induced by the map. We thus expect an increase in ρ_1 as a function of noise intensity. This is shown in Figure 4, where noise activates the deterministic properties of the map. The value of ρ_1 has already been linked to the detectability of weak signals in neurons as well as their information transfer capabilities (Chacron et al., 2001a).

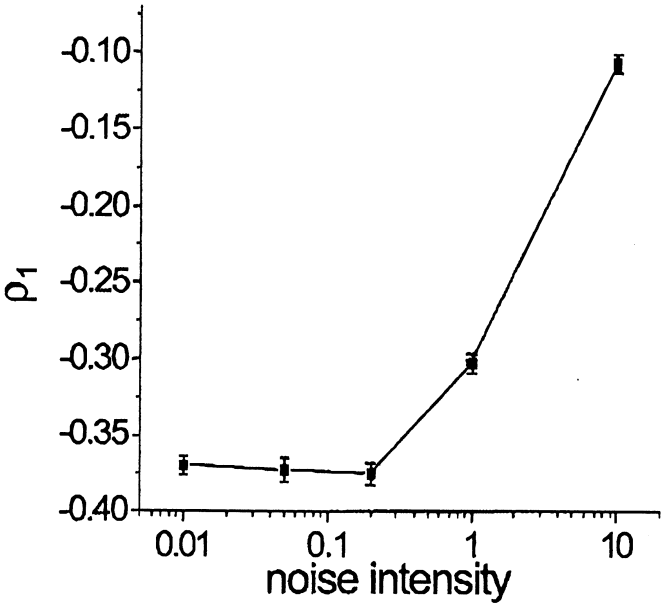

Figure 4: ρ_1 as a function of the noise standard deviation. ρ_1 exhibits a minimum for the noise intensity around 0.2. It is at this noise level that the noise is most effective at perturbing the map without itself destroying the ISI correlations. Parameter values were the same as in Figure 3 with $\alpha = 1$. Twenty thousand ISIs were used in each case.

To understand how the deterministic properties of the map can give rise to ISI correlations in the presence of noise, we study the response of the model to perturbations without noise ($\sigma = 0$). We assume that the stationary regime has been reached, that the model fires periodically, and that a single sufficiently large pulsatile stimulation is delivered a time lapse $\theta < \Delta$ after a discharge, to make the neuron fire ahead of time. This results in a shortened ISI with length θ, and consequently the postdischarge threshold $S(\theta^+)$ is larger than S^*. Following the perturbation, the sequence S_n progressively decreases toward S^*. Given that the interspike interval $\Delta(S)$ is a monotonic increasing function of S, the sudden increase in S at the time of the perturbation and its progressive decrease indicate that the shortened interval is followed by one that is longer than the period and that subsequent intervals progressively decrease toward the stationary value. If the system returns quasi-instantaneously to equilibrium, then only ρ_1 will be significantly negative. However, if the system takes a long time to return to equilibrium after the perturbation, then coefficients at higher lags can also be negative. We concentrate on the regime at which

the voltage has almost reached its asymptotic value $\mu\tau_v$ before a firing: this occurs when $\tau_s \gg \tau_v$. We start from equation 3.3 in which we set $v(\Delta_{n+1}) = \mu\tau_v$:

$$S(\Delta_{n+1}, S_n^+) = \mu\tau_v. \tag{3.19}$$

The stationary threshold value is then $S^* = s_0 + \alpha\mu\tau_v$, and equation 3.10 gives us the stationary ISI Δ^*:

$$\Delta^* = \tau_s \ln \frac{s_0 + \alpha\mu\tau_v - s_r}{\mu\tau_v - s_r}. \tag{3.20}$$

Let us suppose that a voltage perturbation advances or delays an action potential, thus causing an ISI θ that can be smaller or greater than Δ^*. Then the new value of the threshold immediately after the action potential is given by

$$S_\theta^+ = s_0 + \alpha\left[s_r + (s_0 + \alpha\mu\tau_v - s_r)\exp\left(\frac{-\theta}{\tau_s}\right)\right]. \tag{3.21}$$

The next ISI, in the absence of further perturbations, will then be given by

$$\theta_{next} = \tau_s \ln\left\{\frac{S_\theta^+ - s_r}{\mu\tau_v - s_r}\right\}. \tag{3.22}$$

Equations 3.21 and 3.22 give us the relation between θ_{next} and θ:

$$\theta_{next} = \tau_s \ln\left\{\frac{s_0 - s_r + \alpha[s_r + (s_0 + \alpha\mu\tau_v - s_r)\exp(-\frac{\theta}{\tau_s})]}{\mu\tau_v - s_r}\right\}. \tag{3.23}$$

The derivative of the map $\theta_{next} = f(\theta)$ is given by

$$f'(\theta) = \frac{-\alpha(s_0 + \alpha\mu\tau_v - s_r)}{s_0 - s_r + \alpha[s_r + (s_0 + \alpha\mu\tau_v - s_r)\exp(-\frac{\theta}{\tau_s})]} \tag{3.24}$$

and is negative for $s_0 > s_r > 0$ and $\alpha\mu\tau_v > 0$. We now consider the effects of α on the ISI θ_{next}. If $\alpha = 0$, we have

$$\Delta^* = \theta_{next} = \tau_s \ln\left\{\frac{s_0 - s_r}{\mu - s_r}\right\}, \tag{3.25}$$

that is, θ_{next} is independent of θ since we have $f'(\theta) = 0$. This is because the system returns instantaneously to equilibrium and there is no memory extending beyond one ISI. We now consider the effects of $\alpha > 0$. θ_{next} increases with decreasing θ. Thus, a perturbation that causes θ larger (smaller)

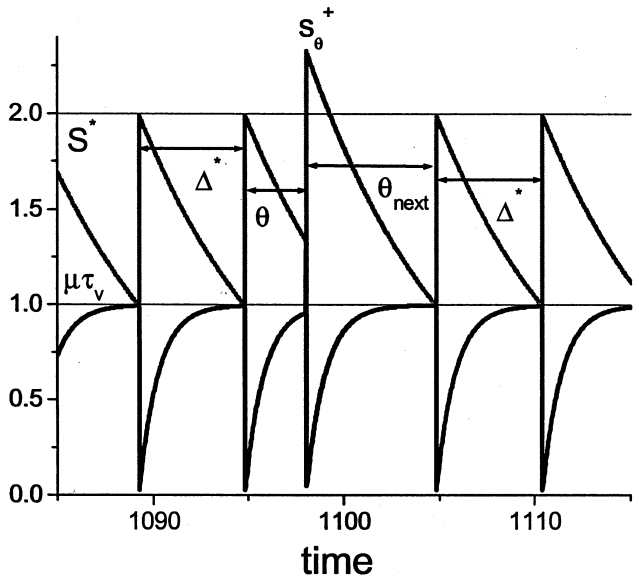

Figure 5: Voltage (black solid line) and threshold (gray solid line) time series. A perturbation in voltage was applied at $t = 1098$. The perturbation caused an action potential to occur earlier than expected. As such, the ISI θ was shorter than Δ^*, and the value of the threshold immediately after that action potential, s_θ^+, was higher than the threshold equilibrium value S^*. Consequently, the threshold took a longer time to decay to μ, and the next ISI θ_{next} was longer than Δ^*. Parameter values were the same as in Figure 4.

than Δ^* will make θ_{next} smaller (larger) than Δ^*. Furthermore, increasing α increases θ_{next}. We illustrate this with numerical examples.

Figure 5 shows a time series in which a perturbation in the voltage was applied at $t = 1099$. The perturbation increased voltage and caused an action potential to occur prematurely. The ISI θ is thus shorter than Δ^* and consequently S_θ^+ (see equation 3.21) is greater than S^*. Since the threshold starts from a higher value, it will take a longer time to decay to the value $\mu\tau_v$. As such, the next ISI θ_{next} will be greater than Δ^*. Similarly, had θ been longer than Δ^*, s_θ^+ would have been smaller than S^*, and consequently θ_{next} would have been smaller than Δ^*. The actual map $\theta_{next} = f(\theta)$ is shown in Figure 6A and has a negative slope as expected. Thus, the deterministic properties of the map lead to a perturbed ISI longer (shorter) than average being followed by an ISI shorter (longer) than average.

Figure 6B illustrates the dependence of θ_{next} on α for different values of θ. As discussed, θ_{next} increases with α. The rate at which θ_{next} increases is, however, greater for low θ than for higher θ. This shows how the determin-

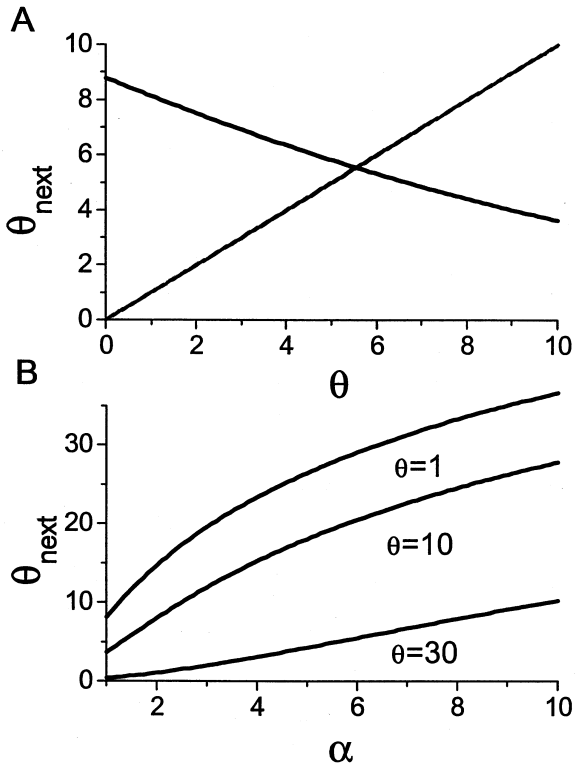

Figure 6: (A) ISI θ_{next} as a function of θ (solid black line). The slope of the map is negative as expected (see the text). (B) ISI θ_{next} as a function of α for different values of θ. Increasing α will increase θ_{next}. Parameters have the same value as in Figure 5 except α.

istic properties of the map in response to perturbations can give rise to ISI correlations in the presence of noise.

3.3 Sinusoidal Stimulation. In this section, we consider the case where the stimulation is sinusoidal $I(t) = \mu + a\sin(\omega t)$, with $a \geq 0$. We show that the response of the LIF with threshold fatigue to such inputs is described by iterates of an annulus map. Such maps can exhibit complex dynamics that can even be chaotic. Through numerical simulations, we illustrate the occurrence of such regimes in the periodically forced LIF with threshold fatigue.

Assuming a firing took place at time t_n, we denote by $v(t, t_n)$ and $s(t, t_n, S_n^+)$ the voltage and threshold at time t, given the initial conditions $v(t_n, t_n) = v_0$ and $s(t_n, t_n, S_n^+) = S_n^+$. Provided $t \geq t_n$ and no discharge takes place on

$[t_n, t]$, we have

$$v(t, t_n) = \mu\tau_v(1-\exp[(t_n-t)/\tau_v]) + \frac{a\tau_v}{1+w^2\tau_v^2}[\sin(wt) - w\tau_v\cos(wt)]$$
$$- \frac{a\tau_v \exp[(t_n - t)/\tau_v]}{1 + w^2\tau_v^2}[\sin(wt_n) - w\tau_v\cos(wt_n)] \quad (3.26)$$

$$s(t, t_n, S_n^+) = s_r + (S_n^+ - s_r)\exp\left(\frac{t_n - t}{\tau_s}\right). \quad (3.27)$$

If $\mu\tau_v + a\tau_v/\sqrt{1+\omega^2\tau_v^2} \leq s_r$, then $v(t, t_n) < s(t, t_n, S_n^+)$ for all $t \geq t_n$ (i.e., no substained firing occurs), and, conversely, if

$$\mu\tau_v + a\tau_v/\sqrt{1+\omega^2\tau_v^2} > s_r, \quad (3.28)$$

then there exists some finite t_{n+1}, with $t_{n+1} > t_n$ such that $v(t_{n+1}, t_n) = s(t_{n+1}, t_n, S_n^+)$. In other words, the inequality 3.28 is a necessary and sufficient condition for sustained firing of the model. When this inequality holds, the LIF with threshold fatigue will generate an infinite sequence of firing times $\{t_i\}_{i=1}^{\infty}$ with $t_n \to \infty$ as $n \to \infty$. We will assume that this is the case throughout the remainder of this section.

The condition for sustained firing is independent of the initial voltage and threshold values; however, the sequence of discharge times depends on these quantities. In the following, we describe the relation between successive discharge times and postdischarge thresholds through the construction of an annulus map.

The firing time t_{n+1} is given by

$$t_{n+1} = F_1(t_n, S_n^+) \stackrel{def}{=} \inf\{t\colon\ t > t_n, v(t, t_n) = s(t, t_n, S_n^+)\}, \quad (3.29)$$

and the threshold S_{n+1}^+ immediately after the firing is given by

$$S_{n+1}^+ = F_2(t_n, S_n^+) \stackrel{def}{=} s_0 + W(s_r + (S_n^+ - s_r)e^{\frac{t_{n+1}-t_n}{\tau_s}}, \alpha). \quad (3.30)$$

We define the discharge map as $F\colon\ (t_n, S_n^+) \to (t_{n+1} = F_1(t_n, S_n^+), S_{n+1}^+ = F_2(t_n, S_n^+))$ on $[0, \infty) \times [s_0 + W(s_r, \alpha), s_0 + W(V_M, \alpha)]$, where $V_M = \mu\tau_v + a\tau_v/\sqrt{1+\omega^2\tau_v^2}$.

For neural computation, it is of interest to know where spikes occur in relation to periodic forcing (see Hopfield, 1995). Given that the input current I is T-periodic with $T = 2\pi/\omega$, we thus define the firing phase $\phi_n \in [0, 2\pi)$ as

$$\phi_n = w\left\{t_n - T\text{int}\left[\frac{t_n}{T}\right]\right\}, \quad (3.31)$$

where the int[.] denote the integer part.

We can thus associate to F a map $f = (f_1, f_2)$ on the annulus $[0, 2\pi) \times [s_0 + W(s_r, \alpha), s_0 + W(V_M, \alpha)]$ as

$$f_1(\phi_n, S_n^+) = \frac{2\pi}{T} F_1\left(\frac{T}{2\pi}\phi_n, S_n^+\right) \text{ modulo } T \tag{3.32}$$

$$f_2(\phi_n, S_n^+) = F_2\left(\frac{T}{2\pi}\phi_n, S_n^+\right). \tag{3.33}$$

The behavior of the periodically forced LIF with threshold fatigue is completely characterized by the iterates of the discharge map F and its associated annulus map f, in the sense that given the initial discharge time t_1 and the corresponding postdischarge threshold S_1^+, the following discharge times and postdischarge thresholds are determined iteratively as $(t_{n+1}, S_{n+1}^+) = F(t_n, S_n^+)$. We will concentrate on the annulus map f and the sequence of firing phases and postdischarge thresholds $(\phi_i, S_i^+)_{i=1}^{\infty}$. When $\alpha = 0$, the postdischarge threshold is always set to s_0, so that the annulus map reduces to a map on the circle of radius s_0. Furthermore, when $s_r = s_0$, that is, when dealing with the standard LIF without threshold fatigue, this circle map, when restricted to its range, is orientation preserving (Pakdaman, 2001). In such a situation, the system can mainly display phase locking and quasiperiodic behavior, as well as strange nonchaotic dynamics on a parameter set of zero measure. It cannot produce chaos (Coombes, 1999). However, when $\alpha > 0$, no such restrictions hold. Although we did not observe chaotic behavior with $W = W_1$ for the region of parameter space considered in this article, it is possible to observe sensitivity to initial conditions and chaotic dynamics when a nonlinear form is taken for W. We observed chaotic behavior when we chose $W(s, \alpha) = W_2(s, \alpha) \equiv \exp(\alpha s) - 1$ (data not shown). Through systematic numerical simulations, we have observed that such dynamics can be easily observed when α is large and that the sensitivity to initial conditions is associated with a positive leading Lyapunov exponent. The details of this analysis will be described in another study (Chacron, Pakdaman, & Longtin, 2002).

4 Discussion

In this study, we have shown that a simple single neuron model that accounts for the memory seen in several classes of neurons has surprisingly rich dynamical behavior. Previous studies involved either $\alpha = 0$ (Geisler & Goldberg, 1966; Kretzberg, Egelhaaf, & Warcheza, 2001) or $\alpha = 1$ (Geisler & Goldberg, 1966; Holden, 1976; Vibert et al., 1994; Pakdaman & Vibert, 1995; Pakdaman et al., 1996; Chacron et al., 2000, 2001a, 2001b; Liu & Wang, 2001). We instead varied $\alpha \in [0, \infty)$ continuously and studied its effects.

Different values for the parameter α (measuring the amount of memory in the system) gave rise to qualitatively different regimes. The rate and degree of adaptation to a step in current were shown to vary with α. Adaptation is commonly seen in biological neurons; we have found that this interesting

feature could be reproduced by our model and that the rate of adaptation depended on the amount of memory. Another common feature of biological neurons is the saturation in firing rate as the input current is increased. Our model reproduces this feature when $\alpha > 1$, in contrast with the LIF neuron for which the firing rate diverges as a function of the input current. In experimental recordings, this saturation is usually thought to be associated with an absolute refractory period or network effects. Our results show that an absolute refractory period is not necessary to obtain such an effect. In fact, this prediction could be verified experimentally in vitro if the firing-rate saturation due to adaptation is lesser than the firing-rate saturation due to the absolute refractory period.

Under the influence of perturbations and noise, we have shown that the model could give rise to negative ISI interval correlations. The value and rate of decay of these correlations depend on the parameter α and on the noise strength and can be varied to give rise to very different regimes. Expressions were derived for the ISI correlation coefficients. The model was also shown to give rise to ISI correlations similar to those seen in experimental data (Longtin & Racicot, 1998; Chacron et al., 2000). Further, the value of the correlation coefficient at lag 1 was shown to increase as a function of noise intensity. These correlations were shown to increase the detectability of weak signals in neurons (Chacron et al., 2001a). There thus might be an optimal noise intensity at which signal detection is maximal.

ISI correlations have been observed in experimental data taken from neurons in different sensory systems. The advantages of a negative correlation coefficient at lag 1 for stimulus detection through long-term spike train regularization as well as stimulus encoding have been outlined in another study (Chacron et al., 2001a). Moreover, a similar firing mechanism has already been used successfully to model electroreceptors of weakly electric fish that display this negative serial correlation coefficient at lag 1 (Longtin & Racicot, 1998; Chacron et al., 2000, 2001a, 2001b) and could potentially be used to model other neurons that also display negative ISI correlations (Kuffler et al., 1957; Goldberg et al., 1964; Geisler & Goldberg, 1966). In fact, models similar to our own have already been used to model several classes of neurons in the visual system (Keat, Reinagel, Reid, & Meister, 2001), cortical neurons (Liu & Wang, 2001), and electroreceptor afferents (Brandman & Nelson, 2002).

Results similar to our own can be obtained by having adaptation in the reset value of the membrane potential. Geisler and Goldberg (1966) have shown that an adapting reset could give rise to ISI correlations. However, as mentioned, there is experimental evidence for the threshold to firing being dependent on the spiking history (Azouz & Gray, 1999), while there is, to our knowledge, no such evidence for the reset value. We thus believe a dynamic threshold to be more physiologically realistic than a dynamic reset.

Although our model contains two timescales, it cannot reproduce the bursting dynamics seen in many neurons with the parameter range considered in this study. This is because we considered only threshold fatigue after an action potential and not facilitation. Our model is thus different from the integrate-and-fire-or-burst model considered by Coombes, Owen, & Smith (2001), which also has two timescales. It has, however, been shown that the addition of a facilitation current to our model with $\alpha = 1$ could give rise to bursting dynamics (Chacron et al., 2001b).

The response of the model to perturbations and noise will carry over in the presence of sinusoidal forcing (Chacron et al., 2000). However, it is then impossible to obtain analytical explicit expressions for the ISI under voltage perturbations. Furthermore, under sinusoidal forcing, we have shown that our model could be described by a map defined on an annulus. While this may seem a simple extension of the many studies that have described the dynamics of sinusoidally forced standard LIFs by circle maps (Rescigno et al., 1970; Keener et al., 1981; Coombes & Bressloff, 1999; Pakdaman, 2001), it has major implications in terms of the dynamics of the system. Indeed, the circle map associated with the periodically forced standard LIF is one-to-one and orientation preserving, so that it produces only one of the three following regimes: phase locked, quasi-periodic, or strange nonchaotic behavior (Keener, 1980). For fixed parameters, it can produce neither a mix of these nor chaos. In contrast, the annulus map associated with the LIF model with threshold fatigue is not constrained by such limitations and may very well lead to more complex dynamics (Le Calvez, 2000), in agreement with our numerical investigations (details will be described in a future work).

Also, introducing threshold fatigue as in our model yields an adapting sequence of ISIs in the presence of periodic forcing. In contrast, for a step increase in bias current, models in which periodic forcing is taken into account by sinusoidally modulating the threshold or the voltage reset value see an abrupt change in ISI. It should be noted that the annulus map is dissipative and not conservative in general. This system is thus different from the so-called standard map studied by various authors (e.g., Meiss, 1992). Our results suggest that neurons with strong adaptation are more prone to displaying complex dynamics than those that either do not adapt or adapt more slowly. Such sensitivity to initial conditions may confer some advantages, as chaotic systems have the potential to transmit much more information about time-varying stimuli than nonchaotic ones, depending on the Lyapunov exponents of the system (Abarbanel, 1996). Further studies are needed to investigate such possible functional roles of chaos in signal processing in nervous systems.

In this study, we have considered how the addition of threshold fatigue affected the spike train of a single LIF neuron. However, it is clear that adaptation and ISI correlations could also be due to network or synaptic dynamics. To expand on this point, we now discuss the possible biological mechanisms that the threshold fatigue could model.

Cumulative inactivation of sodium channels (Mickus, Jung, & Spruston, 1999) could, for example, give rise to neural adaptation and ISI correlations. However, a fast spike-activated slowly inactivating negative current could also give rise to similar effects: a likely candidate would be members of the KV family of potassium currents (Wang, Gan, Forsythe, & Kaczmarek, 1998). Another candidate could be a calcium-activated potassium current such as I_{ahp}. This current was shown to be present in cortical neurons (Madison & Nicoll, 1984). Liu and Wang (2001) have shown that a model with an I_{ahp} current was qualitatively equivalent to our threshold fatigue model with $W = W_1$ (i.e., a linear threshold reset) and $\alpha = 1$. It is further known that most ionic currents have voltage-dependent conductances. The parameter s_0 represents the amount of reset that is voltage independent. The parameter α in our model could then represent the degree of dependence on the past firing time in the ionic channel that the dynamic threshold models. Increasing α would thus lead to a more history-dependent conductance.

Long-term depression at a synapse could also give rise to relative refractoriness (Hausser & Roth, 1997). In fact, a depressing synapse produces negative spike train correlations (Goldman, Maldonado, & Abbott, 2002). Our model thus bears some similarity with models of short-term plasticity (Fuhrman, Segev, Markram, & Tsodyks, 2002; Goldman et al., 2002). Furthermore, it is known that many synapses are voltage dependent. The parameter α in our model could then represent the voltage dependence of synaptic depression. It should, however, be noted that the recovery time constant of the neurotransmitter at typical synapses is usually in the range of hundreds, if not thousands, of milliseconds (von Gernsdoff, Schneggenburger, Weis, & Neher, 1997). Although neural adaptation usually occurs on much shorter timescales, our model could in principle still be used to account for such phenomena if the threshold time constant is sufficiently long. Moreover, it has been observed that neural adaptation was in many ways similar to recurrent inhibition (Ermentrout, Pascal, & Gutkin, 2001). Our single-neuron model could therefore describe network effects.

It has thus been shown that threshold fatigue can be similar to recurrent inhibition, synaptic depression, or an intrinsic I_{ahp} current responsible for adaptation.

Acknowledgments

We thank C. Laing, B. Doiron, J. Benda, B. Lindner, and L. Maler for useful discussions. This research was supported by NSERC (M. J. C. and A. L.).

References

Abarbanel, H. D. I. (1996). *Analysis of observed chaotic data*. New York: Springer-Verlag.

Abbott, L. F., & Dayan, P. (1999). The effect of correlated variability on the accuracy of a population code. *Neural Comp., 11*, 91–101.

Adrian, E. D., & Zotterman, Y. (1926) The impulse produced by sensory nerve endings. Part 2: The response of a single end-organ. *J. Physiol. (Lond.), 61*, 151–171.

Alstrøm, P., & Levinsen, M. T. (1988). Phase-locking structure of "integrate-and-fire" models with threshold modulation. *Phys. Lett. A, 128*, 187–192.

Azouz, R., & Gray, C. M. (1999). Cellular mechanisms contributing to response variability of cortical neurons in vivo. *J. Neurosci., 19*, 2209–2223.

Brandman, R., & Nelson, M. E. (2002). A simple model of long-term spike train regularization. *Neural Comp., 14*, 1507–1544.

Chacron, M. J., Longtin, A., & Maler, L. (2001a). Negative interspike interval correlations increase the neuronal capacity for encoding time dependent stimuli. *J. Neurosci., 21*, 5328–5343.

Chacron, M. J., Longtin, A., & Maler, L. (2001b). Simple models of bursting and non-bursting P-type electroreceptors. *Neurocomputing, 38*, 129–139.

Chacron, M. J., Longtin, A., St.-Hilaire, M., & Maler, L. (2000). Suprathreshold stochastic firing dynamics with memory in P-type electroreceptors. *Phys. Rev. Lett., 85*, 1576–1579.

Chacron, M. J., Pakdaman, K., & Longtin, A. (2002). *Chaotic firing in the sinusoidally forced leaky integrate and fire model with threshold fatigue*. Unpublished manuscript.

Coombes, S. (1999). Lyapunov exponents and mode-locked solutions for integrate-and-fire dynamical systems. *Phys. Lett. A., 255*, 49–57.

Coombes, S., & Bressloff, P. C. (1999). Mode locking and Arnold tongues in integrate-and-fire neural oscillators. *Phys. Rev. E., 60*, 2086–2096.

Coombes, S., Owen, M. R., & Smith, G. D. (2001). Mode locking in a periodically forced integrate-and-fire-or-burst neuron model. *Phys. Rev. E, 64*, 041914.

Ermentrout, B., Pascal, M., & Gutkin, B. (2001). The effects of spike frequency adaptation and negative feedback on the synchronization of neural oscillators. *Neural Comp., 13*, 1285–1310.

Fuhrmann, G., Segev, I., Markram, H., & Tsodyks, M. (2002). Coding of temporal information by activity-dependent synapses. *J. Neurophysiol., 87*, 140–148.

Geisler, C. D., & Goldberg, J. M. (1966). A stochastic model of the repetitive activity of neurons. *Biophys. J., 7*, 53–69.

Gerstner, W., & van Hemmen, J. L. (1992). Associative memory in a network of "spiking" neurons. *Network, 3*, 139–164.

Glass, L., & Mackey, M. C. (1979). A simple model for phase locking of biological oscillators. *J. Math. Biol., 7*, 339–352.

Goldberg, J. M., Adrian, H. O., & Smith, F. D. (1964). Response of neurons of the superior olivary complex of the cat to acoustic stimuli of long duration. *J. Neurophysiol., 27*, 706–749.

Goldman, M. S., Maldonado, P., & Abbott, L. F. (2002). Redundancy reduction and sustained firing with stochastic depressing synapses. *J. Neurosci., 22*, 584–591.

Hausser, M., & Roth, A. (1997). Dendritic and somatic glutamate receptor channels in rat cerebellar Purkinje cells. *J. Physiol. (Lond.), 501*, 77–95.

Hodgkin, A. L., & Huxley, A. F. (1952). A quantitative description of membrane current and its application to conduction and excitation in nerve. *J. Physiol. (Lond.), 117*, 500–544.

Holden, A. V. (1976). *Models of the stochastic activity of neurones*. New York: Springer-Verlag.

Hopfield, J. J. (1995). Pattern recognition computation using action potential timing for stimulus representation. *Nature, 376*, 33–36.

Keat, J., Reinagel, P., Reid, R. C., & Meister, M. (2001). Predicting every spike: A model for the response of visual neurons. *Neuron, 30*, 803–817.

Keener, J. P. (1980). Chaotic behavior in piecewise continuous difference equations. *Trans. Amer. Math. Soc., 261*, 589–604.

Keener, J. P., Hoppensteadt, F. C., & Rinzel, J. (1981). Integrate-and-fire models of nerve membrane response to oscillatory input. *SIAM J. of Appl. Math., 41*, 816–823.

Kreztberg, J., Egelhaaf, M., & Warzecha, A. K. (2001). Membrane potential fluctuations determine the precision of spike timing and synchronous activity: A model study. *J. Comput. Neurosci., 10*, 79–97.

Kuffler, S. W., Fitzhugh, R., & Barlow, H. B. (1957). Maintained activity in the cat's retina in light and darkness. *J. Gen. Physiol., 40*, 683–702.

Lansky, P., & Sato, S. (1999). The stochastic diffusion models of nerve membrane depolarization and interspike interval generation. *J. Peripher. Nerv. Syst., 4*, 27–42.

Le Calvez, P. (2000) *Dynamical properties of diffeomorphisms of the annulus and of the torus*. Providence, RI: American Mathematical Society.

Liu, Y. H., & Wang, X. J. (2001). Spike frequency adaptation of a generalized leaky integrate-and-fire neuron. *J. Comput. Neurosci., 10*, 25–45.

Longtin, A., & Racicot, D. M. (1998). Spike train patterning and forecastability. *Biosystems, 40*, 111–118.

MacGregor, R. J., & Lewis, E. R. (1977). *Neural modeling*. New York: Plenum Press.

Madison, D. V., & Nicoll, R. A. (1984). Control of the repetitive discharge of rat CA1 pyramidal neurones in vitro. *J. Physiol., 354*, 319–331.

Mickus, T., Jung, H. Y., & Spruston, N. (1999). Properties of slow cumulative sodium channel inactivation in rat hippocampal CA1 pyramidal neurons. *Biophys. J., 76*, 846–860.

Meiss, J. D. (1992). Symplectic maps, variational principles, and transport. *Rev. Mod. Phys., 64*, 795–848.

Neiman, A., & Russell, D. F. (2001). Stochastic biperiodic oscillations in the electroreceptors of paddlefish. *Phys. Rev. Lett., 86*, 3443–3446.

Pakdaman, K. (2001). The periodically forced leaky integrate-and-fire model. *Phys. Rev. E., 63*, 1907–1912.

Pakdaman, K., Tanabe, S., & Shimokawa, T. (2001). Coherence resonance and discharge time reliability in neurons and neuronal models. *Neural Networks, 14*, 895–905.

Pakdaman, K., & Vibert, J. F. (1995). Modeling excitatory networks. *Journal of Sice, 34*, 788–793.

Pakdaman, K., Vibert, J. F., Boussard, E., & Azmy, N. (1996). Single neuron with recurrent excitation: Effect of the transmission delay. *Neural Networks, 9*, 797–818.

Panzeri, S., Petersen, R. S., Schultz, S. R., Lebedev, M., & Diamond, M. E. (2001). The role of spike timing in the coding of stimulus location in rat somatosensory cortex. *Neuron, 29*, 769–777.

Reiss, R. F. (1962). A theory and simulation of rhythmic behavior due to reciprocal inhibition in small nerve nets. *Proceedings of the 1962 AFIPS Spring Joint Computer Conference, 21*, 171–194.

Rescigno, A., Stein, R. B., Purple, R. L., and Popele, R. E. (1970). A neuronal model for the discharge patterns produced by cyclic inputs. *Bull. Math. Biophys., 32*, 337–353.

Ricciardi, L. M., Di Crescenzo, D., Giorno, V., & Nobile, A. G. (1999). An outline of theoretical and algorithmic approaches to first passage time problems with applications to biological modelling. *Mathematica Japonica, 50*, 247–322.

Schäfer, K., Braun, H. A., Peters, C., & Bretschneider, F. (1995). Periodic firing pattern in afferent discharges from electroreceptor organs of catfish. *Eur. J. Physiol., 429*, 378–385.

Segundo, J. P., Perkel, D. H., Wyman, H., Hegstad, H., & Moore, G. P. (1968). Input output relations in computer simulated nerve cells. *Kybernetik, 4*, 157–175.

Stein, R. B. (1965). A theoretical analysis of neuronal variability. *Biophys. J., 5*, 173–194.

Teich, M. C., & Lowen, S. B. (1994). Fractal patterns in auditory nerve spike trains. *IEEE Eng. Med. Biol. Mag., 13*, 197–202.

Tiesinga, P. H. E., Fellous, J. M., José, J. V., & Sejnowski, T. J. (2002). Information transfer in entrained cortical neurons. *Network, 13*, 41–66.

Treves, A. (1996). Mean-field analysis of neuronal spike dynamics. *Network, 4*, 259–284.

Tuckwell, H. C. (1988). *Introduction to theoretical neurobiology: I.* Cambridge: Cambridge University Press.

Vibert, J. F., Pakdaman, K., & Azmy, N. (1994). Inter-neural delay modification synchronizes biologically plausible neural networks. *Neural Networks, 7*, 589–607.

von Gernsdoff, H., Schneggenburger, R., Weis, S., & Neher, E. (1997). Presynaptic depression at a calyx synapse: The small contribution of metabotropic glutamate receptors. *J. Neurosci., 17*, 8137–8146.

Wang, L. Y., Gan, L., Forsythe, I. D., & Kaczmarek, L. K. (1998). Contribution of the Kv3.1 potassium channel to high-frequency firing in mouse auditory neurones. *J. Physiol. Lond., 509*, 183–194.

Weiss, T. F. (1966). A model of the peripheral auditory system. *Kybernetik, 3*, 153–175.

Wehmeier, W., Dong, D., Koch, C., & van Essen, D. (1989). Modeling the mamalian visual system. In C. Koch & I. Segev (Eds.), *Methods in neuronal modeling*. Cambridge, MA: MIT Press.

Wilson, D. M., & Waldron, I. (1968). Models for the generation of the motor output pattern in flying locusts. *Proceedings IEEE, 56*, 1058–1064.

Yamamoto, A., & Nakahama, H. (1983). Stochastic properties in somatosensory cortex and mesencephalic reticular formation during sleep-waking states. *J. Neurophysiol., 49*, 1182–1198.

Received April 9, 2002; accepted July 8, 2002.